Moisture Permeability Through Multilayered Barrier Films as Applied to Flexible OLED Display

J. Greener,* K. C. Ng, K. M. Vaeth, T. M. Smith

Eastman Kodak Company, Rochester, New York 14650-2158

Received 27 February 2007; accepted 29 March 2007
DOI 10.1002/app.26863
Published online 28 August 2007 in Wiley InterScience (www.interscience.wiley.com).

ABSTRACT: Strict protection of organic light-emitting diodes (OLEDs) and other optoelectronic materials from direct contact with ambient moisture and oxygen is one of the major challenges in the development of flexible OLED displays and other flexible electronic devices. This problem is typically addressed by the use of polymeric substrates with multilayered barrier coatings comprising alternating organic/inorganic layers. The multilayered barrier approach is critically examined using a numerical model based on a defect-dominated diffusion process combined with experiments involving face-to-face lamination of two barrier films. The modeling results identify two regimes, corresponding to two distinct permeation mechanisms, and provide scaling relationships and general design criteria for multilayered barrier coatings. The results suggest that the most significant gain in barrier performance can be realized when the thickness of the organic/adhesive layer(s) in the multilayered structure is less than the average pinhole (defect) size in the inorganic barrier layer(s). © 2007 Wiley Periodicals, Inc. J Appl Polym Sci 106: 3534–3542, 2007

Key words: OLED; barrier; film; WVTR; permeability

INTRODUCTION

One of the major challenges in the development of flexible organic light-emitting diode (OLED) devices is the need to protect the OLED materials from damage by ambient moisture and oxygen. These devices require protective layers and encapsulants with extremely low moisture and oxygen permeabilities; moisture permeability of less than 10^{-6} g/m^2/day and oxygen permeability of less than 10^{-3} cc/m^2/day are generally cited as the minimum values required to assure adequate lifetime stability for most OLED devices.[1] Polymeric materials, however, are inherently porous, having moisture permeabilities typically > 1 g/m^2/day, and are therefore not suitable, in themselves, to provide adequate protection to the OLED materials. One way to lower the permeability of the polymeric substrate is to coat it with an essentially impermeable inorganic layer via an appropriate vacuum deposition process. Such layers, usually comprising oxides, nitrides, or carbides, are impermeable to moisture and oxygen only if the layer is free of defects. However, defects (''pinholes'') are inherently present in vacuum-deposited layers because of imperfections in the deposition process (*intrinsic* defects) or as a result of the presence of impurities in the vacuum chamber or on the coated substrate (*extrinsic* defects). Thus, even if the substrate is coated with an inorganic barrier layer, the barrier performance of this composite structure is still expected to fall short for OLED applications. General approaches to reduce the number and size of pinholes in inorganic layers include various modifications to the vacuum-deposition process while paying close attention to cleanliness. With these improvements, the permeability can be significantly lowered, but it is still unlikely to meet the OLED targets cited earlier. One approach for boosting the performance of barrier films was pioneered by several companies in the food packaging industry and further developed for OLED applications by a team from Battelle (now licensed and under development by Vitex Corp. and known under the trade name of Barix®). This approach involves the creation of a multilayered stack of inorganic layers separated by thin organic layers (typically UV-curable acrylates), which allegedly creates a so-called ''tortuous path'' for the diffusing species, thereby lowering the overall permeability of the film.[2–4] With this general approach Vitex and others claim water vapor transmission rates (WVTRs) approaching the 10^{-6} g/m^2/day target. However, this method is quite costly and not sufficiently robust. Particularly problematic with this approach are the issues involving acrylate deposition and curing, including control of film thickness, particulate formation in the deposition chamber, and health and safety concerns with the acrylate formulation. A very similar structure can be fabricated by

Correspondence to: J. Greener (jgreener@rohmhaas.com).
**Present address:* Rohm and Haas Electronic Materials, Rochester, New York 14650.

Journal of Applied Polymer Science, Vol. 106, 3534–3542 (2007)

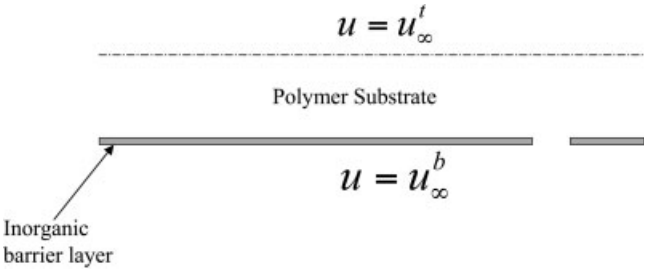

Figure 1 Schematic representation of a barrier film.

laminating two barrier films together to create a multilayered structure similar to the Barix® structure but potentially at a significantly lower cost.

To assess the feasibility and potential of the lamination approach and, more broadly, the multilayered approach, for attaining the challenging barrier requirements for flexible OLED display, we developed a numerical model, based on a defect-dominated diffusion process, to evaluate the moisture permeability through various types of organic–inorganic layered stacks. The model is delineated in the ''Diffusion Model'' Section, and experiments designed to test the computational results are described in the ''Experimental'' Section. The modeling and experimental results are presented in the ''Results and Discussion'' Section, and their implications for future opportunities with this approach are discussed in the ''Summary'' Section.

DIFFUSION MODEL

The defect-dominated diffusion modeling framework for describing moisture and gas transport through inorganic barrier layers was first proposed by Prins and Hermans.[5] Simply stated, this approach assumes that water or gas molecules can traverse within an inorganic layer only through existing defects or pinholes. Thus, for the purposes of this analysis, this layer is taken to be infinitesimally thin and is characterized by a nominal defect (pinhole) size, L_h, and an average pinhole density N_d ($\approx$ pinholes/unit area), which is directly related to the average distance between pinholes, L_d. For simplicity, the defects are represented by ''virtual holes'' with an average size (diameter), L_h, which corresponds to the rate of moisture transport through the defect; the larger the value of L_h, the higher the permeation rate through the layer. A similar approach was applied in several studies[4–9] to tackle the problem of moisture transport through various barrier layer structures. A schematic representation of the porous barrier layer is shown in Figure 1. L_h and L_d are assumed to be known parameters that define the quality of a given barrier layer. ''Good'' barrier layers, i.e., layers with low moisture or gas permeability, have small L_h and high L_d (or low pinhole density) values. Such layers can be produced by utilizing a deposition process that minimizes intrinsic defects and/or by operating in a ''clean room'' environment to minimize extrinsic defects. Gas transport through any adjacent organic layer (e.g., a polymeric substrate or a coated/laminated layer) follows a given diffusive law. In the present analysis, we assume the diffusion processes in all organic layers to be Fickian.

In the first part of the analysis, we consider a laminate structure of the type shown in Figure 2. In this structure, the two barrier films (barrier film = polymeric substrate coated with an inorganic barrier layer) are laminated face-to-face, i.e., with the two barrier layers joined together by an adhesive layer, as shown. The thickness of the adhesive layer, L_a, and the diffusion coefficient of the adhesive material, D_a, are parameters associated with the lamination process and the adhesive formulation. In the scheme in Figure 2, two adjacent pinholes on both sides of the adhesive layer are shown to be a distance L_d' apart. This length scale represents the average misalignment (''misregistration'') of two defects in two adjacent barrier layers produced by the lamination step, and it is generally not the same as the L_d parameter defined earlier. But these two length scales are closely correlated, so we use the same notation for both parameters, i.e., $L_d \approx L_d'$. The flux [permeability, p, or WVTR, see eq. (7) below] across the laminate structure can be obtained by solving the three-dimensional (3D) diffusion equation with the corresponding boundary conditions,

$$\frac{\partial u}{\partial t} = \frac{\partial}{\partial x}\left(D\frac{\partial u}{\partial x}\right) + \frac{\partial}{\partial y}\left(D\frac{\partial u}{\partial y}\right) + \frac{\partial}{\partial z}\left(D\frac{\partial u}{\partial z}\right) \quad (1)$$

$$\begin{aligned} u &= u_\infty^b \quad \text{at } z = 0 \\ u &= u_\infty^t \quad \text{at } z = L \end{aligned} \quad (2)$$

$$\frac{\partial u}{\partial n} = 0 \qquad \text{at the barrier surface} \quad (3)$$

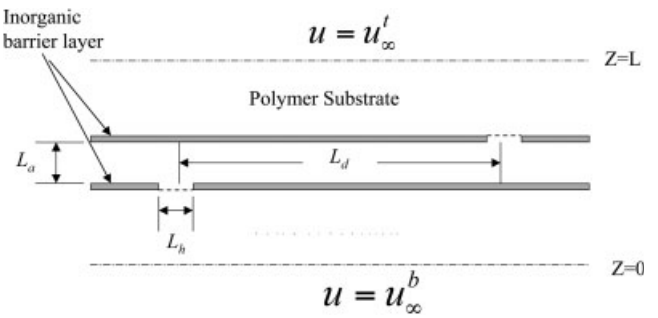

Figure 2 Geometry of a laminate structure [see eqs. (1)–(3) for definitions].

where u is the mass moisture concentration, D is the diffusion coefficient that can vary from layer to layer, u^b_∞ and u^t_∞ are the concentrations at the bottom and top surfaces, respectively, and n is the outward normal to the film surface. Also, as we assume that the barrier film is semi-infinite along the x- and y-axis, edge effects are ignored. At time $t = 0$, $u = 0$ throughout the structure except for the top surface where the moisture level is specified to represent $\sim 100\%$ RH.

Because of the irregular geometry of the laminate structure, the corresponding diffusion problem must be solved numerically. We use a finite-difference scheme with a variable grid to solve this 3D mass transport problem. The computational domain is divided into grid boxes of size (Δx, Δy, Δz), where we denote:

$$\begin{aligned} x_i &= i\Delta x, \qquad i = 0, 1, \ldots, nx \\ y_j &= j\Delta y, \qquad j = 0, 1, \ldots, ny \\ z_k &= k\Delta z, \qquad k = 0, 1, \ldots, nz \end{aligned} \tag{4}$$

Let $u_{i,j,k}$ denote $u(x_i, y_j, z_k)$. For all interior points, the diffusion equation, eq. (1), can be discretized as follows:

$$\begin{aligned} \frac{du_{i,j,k}}{dt} = & \frac{D_{i+1/2,j,k}\left(\frac{u_{i+1,j,k}-u_{i,j,k}}{\Delta x}\right) - D_{i-1/2,j,k}\left(\frac{u_{i,j,k}-u_{i-1,j,k}}{\Delta x}\right)}{\Delta x} \\ & + \frac{D_{i,j+1/2,k}\left(\frac{u_{i,j+1,k}-u_{i,j,k}}{\Delta y}\right) - D_{i,j-1/2,k}\left(\frac{u_{i,j,k}-u_{i,j-1,k}}{\Delta y}\right)}{\Delta y} \\ & + \frac{D_{i,j,k-1/2}\left(\frac{u_{i,j,k+1}-u_{i,j,k}}{\Delta z}\right) - D_{i,j,k-1/2}\left(\frac{u_{i,j,k}-u_{i,j,k-1}}{\Delta z}\right)}{\Delta z} \end{aligned} \tag{5}$$

where $D_{i,j,k} = D(x_i, y_j, z_k)$. At the top surface ($z = L$), $u_{i,j,k} = u^t_\infty$, and at the bottom surface ($z = 0$), $u_{i,j,k} = u^b_\infty$. At the barrier layer, we use the boundary condition of eq. (3) to modify the discretized eq. (5). For example, if the point (x_i, y_j, z_k) is located on the barrier layer and the outward normal is pointing to the increasing z direction, eq. (5) is modified to take the form

$$\begin{aligned} \frac{du_{i,j,k}}{dt} = & \frac{D_{i+1/2,j,k}\left(\frac{u_{i+1,j,k}-u_{i,j,k}}{\Delta x}\right) - D_{i-1/2,j,k}\left(\frac{u_{i,j,k}-u_{i-1,j,k}}{\Delta x}\right)}{\Delta x} \\ & + \frac{D_{i,j+1/2,k}\left(\frac{u_{i,j+1,k}-u_{i,j,k}}{\Delta y}\right) - D_{i,j-1/2,k}\left(\frac{u_{i,j,k}-u_{i,j-1,k}}{\Delta y}\right)}{\Delta y} \\ & + \frac{D_{i,j,k+1/2}\left(\frac{u_{i,j,k+1}-u_{i,j,k}}{\Delta z}\right)}{\Delta z/2} \end{aligned} \tag{6}$$

Thus, we can compute the rate of change of concentration u at every point. We use a standard ordinary differential equation (ODE) solver to solve the corresponding set of ODE's. As we are interested in the steady-state solution ($du/dt = 0$), we can solve the diffusion equation until the solution becomes constant over a given time interval or by setting the left-hand side of eq. (5) equal to zero. In the latter case, we obtain a system of linear equations with the unknowns $u_{i,j,k}$, which can also be solved by a standard linear equation solver. In this scheme, we use a linear equation solver routine to find the steady-state solution. The sought-after WVTR is defined as the average flux at $z = 0$, i.e.,

$$\text{WVTR} = \frac{1}{A}\int\int D\frac{\partial u}{\partial z}dxdy \quad \text{at } z = 0 \tag{7}$$

where A is the area of the bottom surface. Because of the irregular geometry and different length scales involved in the analysis, this computation requires a very large grid of $80 \times 80 \times 80$ and substantial CPU time.

A similar computational scheme is applied to the multilayer structure shown schematically in Figure 3. In this case, the organic layers are typically applied by a coating process of some type rather than by lamination. The thickness of the organic layers for this structure is also designated by L_a.

EXPERIMENTAL

In an attempt to assess the lamination approach and verify the modeling results, we produced a variety of laminate structures and tested their barrier performance. All of the laminate structures comprised one type of barrier film laminated face-to-face (see Fig. 2), using a variety of adhesive formulations. The barrier film selected for this study is GXP® film, obtained from Toppan Corp., which comprises a $\sim$ 12 μm Mylar polyethylene terephthalate (PET) substrate coated with three barrier layers. This film

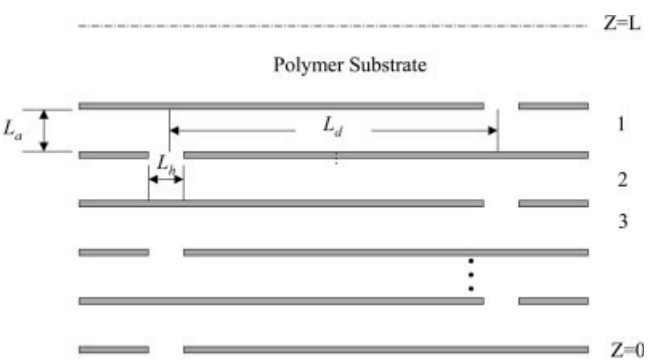

Figure 3 Geometry of a multilayered stack [see eqs. (1)–(3) for definitions].

TABLE I
List of Laminate Structures and Corresponding WVTR's

Lam no.	Adhesive	Adhesive type	Adhesive thickness (μm)	WVTR × 10^{-3} [g/m^2/day]	BIF_L[a]
1	Vitel 3300	Thermal	6	1.2	13.6
2	Cyracure 1[b]	UV	5	1.2	13.6
3	Neorez R-9330	Thermal	2	1.4	11.7
4	Sefrene 2022	Thermal	4	1.1	14.9
5	Sefrene 2022	Thermal	6	1.2	13.6
6	Vitel 3300	Thermal	4	1.3	12.6
7	Cyracure 2[c]	UV	15	0.9	18.2
8	Sefrene 2022[d]	Thermal	3	1.2	13.6
9	Vitel 3300[e]	Thermal	3	1.4	11.7
10	Cyracure 2[c]	UV	8	1.1	14.9
11	Cyracure 2[c]	UV	8	1.4	11.7
12	Cyracure 2[c]	UV	10	1.4	11.7

[a] The WVTR of the unlaminated GXP® barrier film is estimated at 0.0163 [g/m^2/day] based on the Ca test.
[b] Cyracure composition: UVR-6128/UVR-6100/UVI-6100: 66/30/4.
[c] Cyracure composition: UVR-6128/UVR-6100/UVI-6100: 86/10/4.
[d] Sefrene 2022 + 10% colloidal silica.
[e] Vitel 3300 + 10% colloidal silica.

was chosen because of its relatively good barrier performance and its availability in roll form. A variety of adhesives, including thermal, UV, and pressure-sensitive adhesive formulations, were evaluated at various adhesive layer thicknesses (L_a) spanning the range from about 1 to 15 μm. The adhesive formulations were coated manually or by a solvent coating machine on the barrier side of the GXP® film, and then the coated films were laminated face-to-face on a Seal 400 40″ laminator.

The laminated structures were cut and tested for permeability. Because of the generally low permeabilities of the formed laminate structures, the standard MOCON® test method for measuring the WVTR was inadequate, and we had to turn to the more sensitive calcium method. In this method, pioneered by a team from Philips Corp.,[4,10] the amount of moisture or oxygen diffusing into a test cell is monitored by following the oxidation reaction of a reactive metal, such as Mg or Ca, as it comes in contact with moisture and/or oxygen,

$$2M + O_2 + 2H_2O \rightarrow 2M(OH)_2 \quad (M = Mg \text{ or } Ca) \quad (8)$$

Thin films of the metals used in this test have very high optical density (opacity), whereas the films of the corresponding metal hydroxides are relatively transparent. Therefore, water and oxygen permeation can readily be monitored by following the evolution in optical density of the coated metal layer over time. The actual WVTR of the test sample can be estimated from data generated by this technique via a simple procedure described in the Appendix. Some of the laminates produced in this study and the corresponding WVTR's are listed in Table I.

RESULTS AND DISCUSSION

The main object of this study was to identify the conditions whereby the ''tortuous path'' mechanism dominates the permeation process through the multilayered structure such that the WVTR is significantly lowered. To this end, we applied the model to compute the WVTR in various multilayered film structures, covering a wide, though practical, parameter space. The parameters investigated in this study are L_h and L_d (representing the overall quality of the vacuum-deposited barrier layer(s)), L_a (thickness of the adhesive/organic layer), and D_a (representing the constitution/composition of the adhesive/organic layer). L_a was varied over a range of 0.01–100 μm, while the ranges for L_d and L_h were 10–500 μm and 0.1–3 μm, respectively. The diffusion coefficient of the adhesive layer was investigated over the range 10^{-10}–10^{-7}cm^2/s—a typical variation for polymeric materials over a range of ambient temperatures.

Figures 4–6 are plots of WVTR versus L_a, showing the independent effects of L_d, L_h, and D_a on the permeability of moisture for the general laminate structure of Figure 2. In most cases, the contribution of the substrate layer to the overall WVTR is relatively small, assuming the substrate materials have typical polymer permeabilities, although under some conditions the substrate effect can be notable. Over the parameter space covered, the results show very strong effects of L_d and D_a and a somewhat lesser effect of L_h, particularly for $L_a < L_h$. The most significant feature of the computed results is the clear demarcation between laminate structures with $L_a \ll L_h$ and those with $L_a \gg L_h$. If the adhesive layer is thicker than the average pinhole size, the corresponding WVTR is independent to a first-order of L_a, whereas for

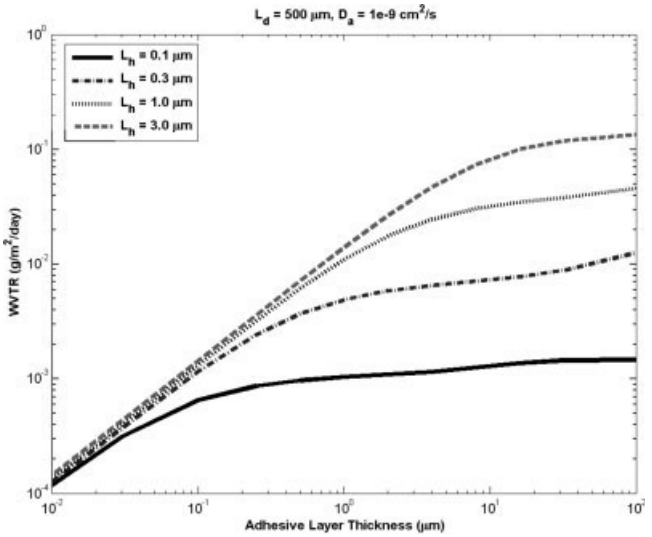

Figure 4 WVTR versus adhesive layer thickness; effect of average pinhole size for a laminate structure with $L_d = 500$ μm and $D_a = 10^{-9}$ cm^2/s.

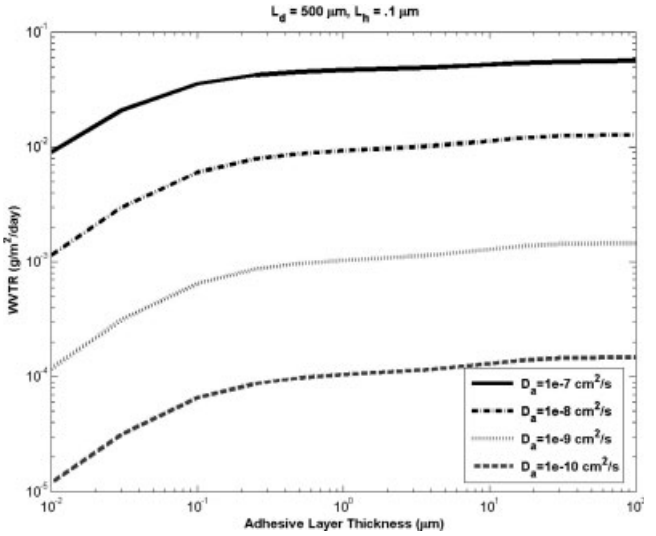

Figure 6 WVTR versus adhesive layer thickness; effect of the diffusion coefficient of the adhesive layer for a laminate structure with $L_h = 0.1$ μm and $L_d = 500$ μm.

$L_a \ll L_h$, the WVTR of the structure increases linearly with L_a in the logarithmic space shown. This feature can be further highlighted by reducing all of the results in Figures 4–6 into a single dimensionless plot, using appropriate scaling. Such a plot is constructed in Figure 7, based on the following scaling relationships:

$$\langle \mathrm{WVTR} \rangle \equiv \mathrm{WVTR} \frac{L_d^2}{D_a \Delta u_\infty L_h} \tag{9a}$$

$$\langle L_a \rangle \equiv \frac{L_a}{L_h} \tag{9b}$$

As shown, the reduced plot can be divided into two distinct regimes. The slightly ''banded'' character of the reduced plot is the result of some computational error (''numerical noise'') caused by the coarseness of the very large finite-difference mesh. In general, however, the scaling suggests that in Regime I ($L_a/L_h < 1$) diffusion through the adhesive layer dominates the permeation process, while in Regime II ($L_a/L_h > 1$), the process is dominated by ''diffusion'' or transport through the pinholes, with the effect of the adhesive layer being relatively small. Thus, an effective tortuous path is established only in Regime I, while the permeation in Regime II corresponds to

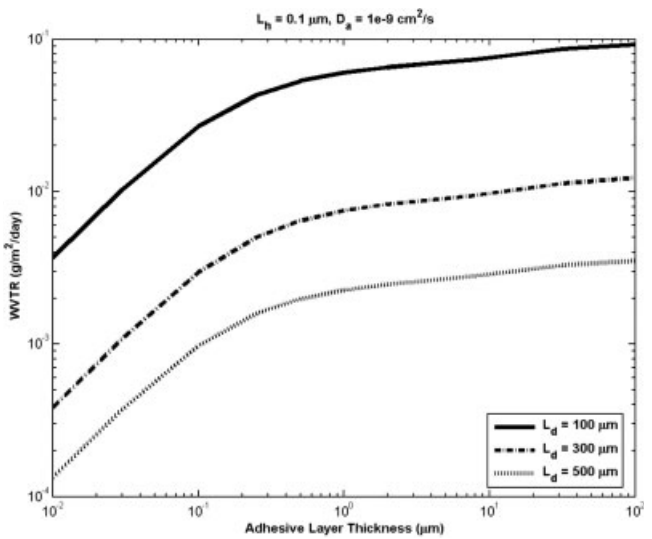

Figure 5 WVTR versus adhesive layer thickness; effect of the average defect-to-defect distance for a laminate structure with $L_h = 0.1$ μm and $D_a = 10^{-9}$ cm^2/s.

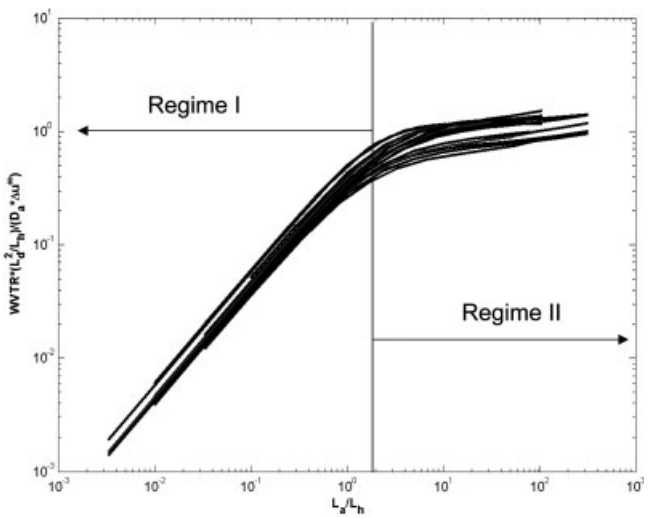

Figure 7 Dimensionless plot of WVTR versus adhesive layer thickness for the laminate structure of Figure 2, based on results in Figures 4–6.

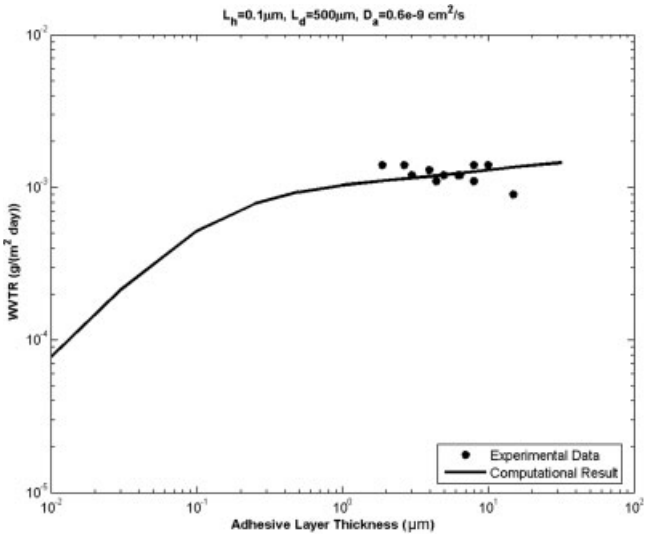

Figure 8 WVTR versus L_a for a laminate structure with the following parameters: L_h = 0.1 μm, L_d = 500 μm, D_a = 0.6×10^{-9} cm^2/s; comparison of modeling results with experimental data.

a straightforward diffusive process through the organic/adhesive layer. Henceforth, we refer to Regime I as the ''Tortuous Path Regime,'' and to Regime II as the ''Diffusive Regime.'' This result clearly suggests that, for a given barrier film, it is desirable to operate within the Tortuous Path Regime, because only in this regime can significant improvement in barrier performance be realized by the lamination process, particularly through changes in the thickness of the adhesive layer. Reductions in pinhole density (increase in L_d) and/or in the diffusion coefficient of the adhesive layer (D_a) can also lead to a significant reduction in the WVTR in both regimes, while decrease in pinhole size (L_h) would be beneficial only in the Diffusive Regime, with only a minor effect in the Tortuous Path Regime. As noted in the ''Introduction'' Section, increase in L_d would require changes in the vacuum deposition process and in the composition of the inorganic barrier layer, whereas changes in D_a can be achieved by variation in the composition and formulation of the adhesive layer. For example, addition of nanoclay particles to the polymeric adhesive matrix can substantially reduce the effective diffusion coefficient of the adhesive layer[11,12] and thereby improve the barrier performance of the laminate structure.

Experimental data for several laminate structures generated in this study are summarized in Table I. The data are compared with modeling results in Figure 8 for a particular combination of parameters. The parameters selected for this comparison are arbitrary and represent a reasonable estimate for the materials used, although a very large number of possible combinations can be used to obtain a good match with the computed results. In fact, although a rigorous test of the model is not possible because we currently lack exact values of L_d and L_h for the GXP® film, and the diffusion coefficients of the various adhesive formulations are unknown, it appears that the data points lie within the Diffusive Regime because the WVTR values of the corresponding structures appear to be insensitive to changes in the thickness of the adhesive layer. The relatively low WVTR for the GXP® film is a result of its multilayered structure. Thus, the L_d and L_h values used for this film are arbitrarily selected to represent its effective barrier performance.

Another way to express the barrier performance of the laminate structure is through the barrier improvement factor (BIF_L) where:

$$BIF_L \equiv \frac{WVTR(film)}{WVTR(lam)} \tag{10}$$

and WVTR (lam) is the WVTR of the laminate structure, while WVTR (film) is the WVTR of the unlaminated barrier film. This quantity increases as the barrier performance of the laminate structure is improved. The results of Figure 4 are replotted in Figure 9 in terms of the barrier improvement factor for the laminate structure, showing, again, the significant improvement in barrier performance for structures with $L_a < L_h$. As indicated in Table I, the BIF values for the experimental laminate structures of this study fall in the range of 10–20, suggesting that lamination of the GXP® film to itself (in a face-to-face mode) can lower its WVTR by a factor of 10–20. More significant improvement should be possible if the thickness of the adhesive layer could be lowered

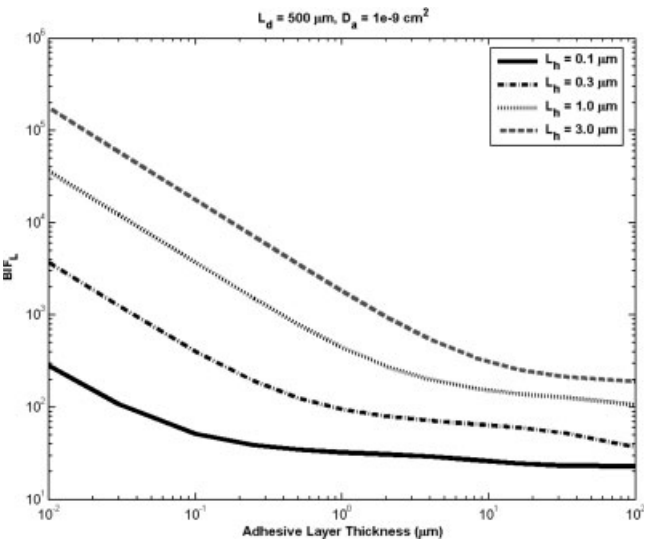

Figure 9 Barrier improvement factor for a laminate structure (Fig. 2) versus adhesive layer thickness; effect of average pinhole size with L_d = 500 μm and D_a = 10^{-9} cm^2/s.

below the L_h value for the GXP® film, but this would require significant improvements in coating capabilities and cleanliness, which was not attempted in this study.

We now turn to the case of the multilayered stack shown schematically in Figure 3. In this case, the effect of adding layered pairs to the structure is simply to lower the WVTR proportionately to the total number of layers or the length of the diffusion path. This is illustrated in Figure 10 where the barrier improvement factor for the multilayered stack (BIF_n) is plotted against the number of layered pairs (n) for two values of the organic layer thickness, L_a. BIF_n for this system is defined as:

$$BIF_n \equiv \frac{WVTR(1)}{WVTR(n)} \tag{11}$$

Thus, the BIF_n for this structure is linearly dependent on the number of layered pairs (n) because of simple additivity of the diffusive path lengths, but the slope of this curve, i.e., the sensitivity of the permeability to change in the number of layers, is strongly related to the particular combination of the parameters L_d, L_h, and L_a. In fact, the general effects of these parameters on the WVTR for the multilayer structure are essentially identical to the case of the laminate structure represented by the results in Figures 4–8. These results can be similarly scaled [eqs. (9a) and (9b)] to produce a master plot of $\langle WVTR \rangle$ versus $\langle L_a \rangle$ shown in Figure 11 for the case of a multilayered structure with $n = 5$. In close analogy to the result for the laminate structure (Fig. 7), the permeation process in this case also involves two regimes corresponding to two permeation mechanisms. Over the parameter space investigated, the results for the multilayered structure suggest that it is possible to improve the WVTR of the barrier film at most by approximately two orders of magnitude when five barrier layers are coated in a single stack. Therefore, for stringent applications, such as flexible OLED displays, a fairly large number of layer pairs may be required and the quality and integrity of each inorganic barrier layer would be critical for achieving the desired low WVTR.

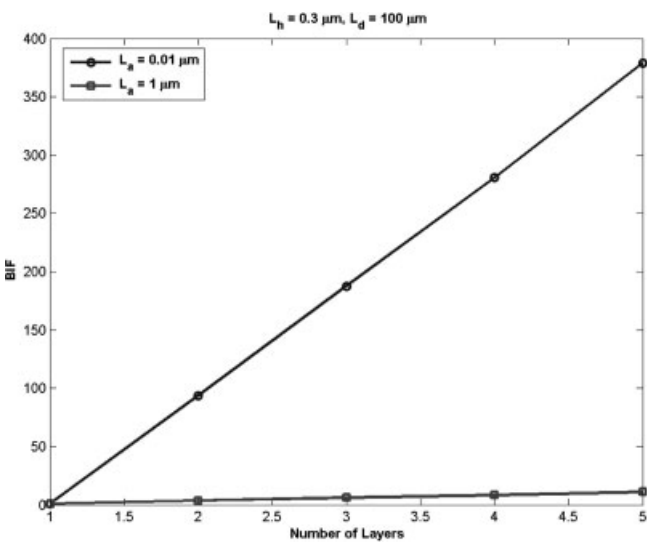

Figure 10 Barrier improvement factor for a multilayer stack (Fig. 3) versus number of layer pairs; effect of organic layer thickness with $L_d = 100$ μm, $L_h = 0.3$ μm and $D_a = 10^{-9}$ cm^2/s.

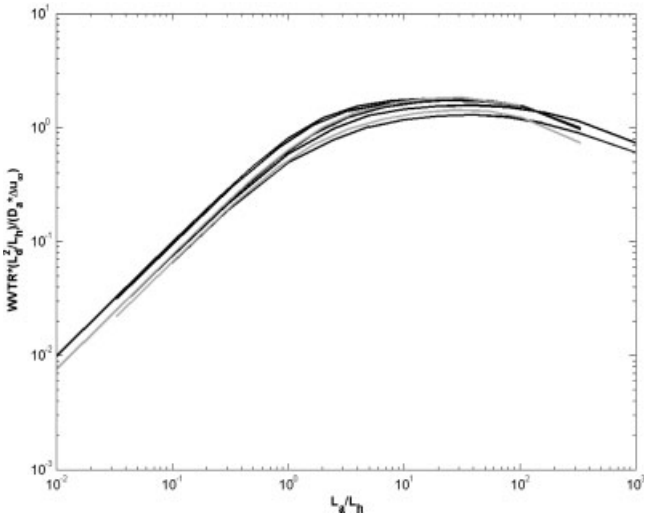

Figure 11 Dimensionless plot of WVTR versus organic layer thickness for the multilayered stack structure of Figure 3 with $n = 5$.

The scaling results for both structures suggest that the WVTR (or moisture flux through the system) can be described by two expressions corresponding to the two operative permeation mechanisms:

$$\text{Regime I}: WVTR \propto D_a \, \Delta u_\infty \frac{L_a}{L_d^2} \; (L_a \ll L_h) \tag{12}$$

$$\text{Regime II}: WVTR \propto D_a \, \Delta u_\infty \frac{L_h}{L_d^2} \; (L_a \gg L_h) \tag{13}$$

In both expressions, L_d^2/D_a represents the nominal diffusion time between two adjacent pinholes located on opposite sides of the organic layer. In Regime I, the mass flux per unit area through the adhesive layer (the most restrictive—''rate-limiting''—section in this regime) is represented by the term $\Delta u_\infty L_a$, while in Regime II, the rate-limiting step is permeation through a pinhole, and $\Delta u_\infty L_h$ is the corresponding mass flux/unit area. These scaling results are useful in gauging the relative effects of the key system parameters on the permeability of the film, and they apply equally to the laminate structure and to the multilayered stack.

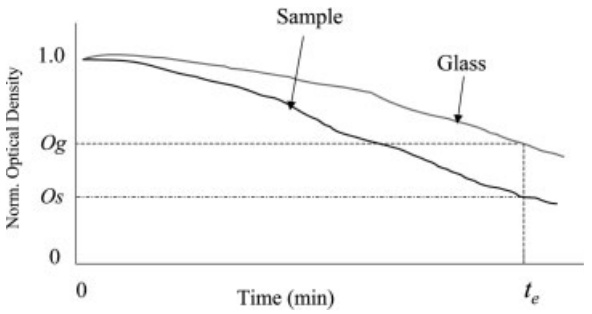

Figure 12 Typical normalized optical density curves for a test sample and a glass benchmark produced by the Ca test.

SUMMARY

The permeation of moisture through a multilayered barrier film, as applied to substrates for flexible OLED displays, was studied experimentally and modeled by numerical simulation of the corresponding diffusion problem. Two multilayered film types were considered in this study: (1) a laminate structure comprising two barrier films laminated face-to-face by an adhesive layer (see Fig. 2), and (2) a multilayered stack comprising a polymeric substrate coated with multiple inorganic/organic layer pairs (see Fig. 3). The latter structure follows a general approach promoted by Vitex Corp. The modeling results clearly identify two diffusion regimes corresponding to two permeation mechanisms for the transport of moisture through a multilayered film. When the adhesive/organic layer thickness is less than the average size of pinholes (defects) in the inorganic barrier layer (Regime I), the permeation process is governed by a ''tortuous path'' mechanism with a strong dependence of the WVTR on the organic layer thickness. When the thickness of the adhesive/organic layer is greater than the average pinhole size (Regime II), the permeation process follows a straightforward diffusive mechanism with the WVTR being only weakly dependent on the organic layer thickness.

These results suggest that the biggest gain in barrier performance can be realized when operating in Regime I where $L_a < L_h$ and when the pinhole size and pinhole density are relatively low. However, to operate in this regime, the organic layers must be very thin (typically, $\ll$1 μm), approaching the limit of conventional coating process capabilities. Furthermore, these layers must be deposited under very clean conditions such that particles greater than $\sim L_a$ must be excluded from the surface or bulk of the organic coating to prevent formation of pinholes and defects within the organic layer. Such tight control on uniformity and cleanliness may be difficult to implement in a roll-to-roll manufacturing operation.

Aside from the thickness of the organic layer, other factors that contribute to the WVTR of the multilayered film are: D_a (the diffusion coefficient of the organic layer), L_h, and L_d [see eqs. (9a) and (9b)]. The latter two parameters are characteristics of the inorganic barrier coating that depend primarily on the composition of the inorganic material and the nature of the vacuum-deposition process. Generally, improvements in the deposition process are expected to reduce the number (density) and size of pinholes, leading to higher L_d and lower L_h, thereby reducing the WVTR of the film. The diffusion coefficient D_a depends mainly on the composition of the adhesive/organic material. As noted in the ''Results and Discussion'' Section, this parameter can be substantially reduced, for example, through formulation of the organic material with nanoclay or other types of discotic nanoparticles.

We thank L. S. Gates, J. DiCillo, M. Licorish, J. Fritch, and K. Landers-Appel for their help with the experimental work. Thanks are also due J. Grace, J. Hammerschmidt, J. Wang, and Y. Rao for useful discussions in the course of this study.

APPENDIX: ESTIMATION OF THE WVTR FROM DATA PRODUCED BY THE Ca METHOD

It was noted in ''Experimental'' Section that, for the very low permeation rates (WVTR $\ll$ 0.01 g/m^2/day) needed in flexible OLED displays, the conventional methods for measuring the WVTR (e.g., via the MOCON® system) are inadequate, and one has to resort to more sensitive detection techniques, such as the Ca method. The Ca method used in this study, produces curves of optical density versus time that follow the conversion of metallic Ca—a nominally opaque material—to transparent $Ca(OH)_2$, as the metal is oxidized by moisture permeating through the test barrier film into an enclosed test cell. Details of the experimental technique can be found elsewhere.[4,10] This technique provides a useful qualitative assessment of the moisture permeability for the test film, but to express the results quantitatively in terms of an effective WVTR, it is necessary to convert the optical density curves generated in this test to the amount of moisture permeating into the cell through the film at a given time.

In estimating this quantity, we make the following assumptions: (1) the Ca layer is fully converted (i.e., through its thickness) to $Ca(OH)_2$, (2) according to eq. (8), 1 mol of H_2O is required to convert 1 mol of Ca to $Ca(OH)_2$, (3) the thickness of the Ca layer in our setup is $\sim$ 50 nm (verified independently), (4) leakage through the seal of the test cell can be ''corrected'' using data for a glass membrane, which is nominally impermeable to moisture (WVTR $\ll 10^{-6}$ g/m^2/day), and (5) the density of metallic Ca at

room temperature is 1550 kg/m^3. With these assumptions, we find:

$$\mathrm{WVTR} \cong 50.2 \frac{O_g - O_s}{t_e O_g} \qquad \text{(A.1)}$$

where O_s is the normalized optical density for the test sample at time t_e (end of the test cycle in min), and O_g is the corresponding fractional optical density for a glass membrane, see Figure 12. Generally, the WVTR values estimated based on this formula are in reasonably good agreement with the MOCON® data when both techniques overlap.

References

1. Langowski, H.-C. Presented at the 47th Annual Technical Conference of the Society of Vacuum Coaters, Dallas, TX, 2004.
2. Affinito, J. D.; Gross, M. E.; Coronado, C. A.; Graff, G. L.; Greenwell, E. N.; Martin, P. M. Thin Solid Films 1996, 290, 63.
3. Affinito, J. D.; Graff, G. L.; Shi, M.-K.; Gross, M. E.; Mounier, P. A.; Hall, M. G. Presented at the 42nd Annual Technical Conference of the Society of Vacuum Coaters, Chicago, IL, 1999.
4. Graff, G. L.; Burrows, P. E.; Williford, R. E.; Praino, R. F. In Flexible Flat Panel Displays; Crawford, G. P., Ed.; Wiley: Chichester, 2005; p 57.
5. Prins, W.; Hermans, J. J. J Phys Chem 1959, 63, 716.
6. Hanika, M.; Langowski, H.-C.; Peuken, W. Presented at the 46th Annual Technical Conference of the Society of Vacuum Coaters, San Francisco, CA, 2003.
7. Jamieson, E. H. H.; Windle, A. H. J Mater Sci 1983, 18, 64.
8. Beu, T. A.; Mercea, P. V. Mater Chem Phys 1990, 26, 309.
9. Rossi, G; Nulman, M. J Appl Phys 1993, 749, 5471.
10. Nisato, G.; Bouten, P. C. P.; Slikkerveer, P. J.; Bennet, W. D.; Graff, G. L.; Rutherford, N.; Wiese, L. In Proceedings of the 21st Annual Asia Display, 8th International Display Workshop, Nagoya, Japan, 2001; p 1435.
11. Nielsen, L. E. J Macromol Sci Chem 1967, 1, 929.
12. Yano, K.; Usuki, A.; Okada, A. J Polym Sci Part A: Polym Chem 1997, 35, 2289.